Phantom experiments with a microwave imaging system for breast-cancer screening

Rubæk, Tonny; Zhurbenko, Vitaliy

Published in:
3rd European Conference on Antennas and Propagation, 2009. EuCAP 2009.

Publication date:
2009

Document Version
Publisher's PDF, also known as Version of record

Phantom Experiments with a Microwave Imaging System for Breast-Cancer Screening

Tonny Rubæk and Vitaliy Zhurbenko
Department of Electrical Engineering
Technical University of Denmark
[tru/vz]@elektro.dtu.dk

***Abstract*—Microwave imaging is emerging as a promising technique for breast-cancer detection. In this paper, the microwave imaging system currently being developed at the Technical University of Denmark is introduced. This system consists of 32 antennas positioned in a cylindrical setup, each equipped with its own transceiver module. The images are reconstructed using a Newton-based algorithm to solve the nonlinear inverse scattering problem.**

***Index Terms*—Biomedical electromagnetic imaging, Cancer, Nonlinear estimation, Microwave imaging**

I. Introduction

Microwave imaging is emerging as a method for breast-cancer detection to supplement the widely used X-ray mammography. The basis for microwave imaging for breast cancer detection is the contrast in electromagnetic constitutive parameters between healthy and cancerous tissue reported by several authors [1]–[3]. This will cause incident electromagnetic waves to scatter if a malignant tumor is present in the breast.

Two different approaches are currently being pursued: Ultrawideband radar-based methods [4]–[6] in which the images are constructed by determining the point-of-origin of reflected pulses, and tomographic or inverse-scattering techniques [2], [7], [8] in which the images are created by solving an inverse scattering problem based on Maxwell's equations and show the distribution of constitutive electromagnetic properties, i.e. permittivity and conductivity.

At the Technical University of Denmark, a microwave imaging system for breast cancer detection is currently being developed. In this system, inverse scattering is applied for creating three-dimensional images from the measured data and 32 antennas, each equipped with their own transceiver module, are used for collecting the measurement data.

In the present paper, the imaging system and imaging algorithm is introduced. This includes an introduction of the measurement setup in Section II, a description of the hardware design in Section III, and a presentation of the imaging algorithm in Section IV.

II. System Setup

The imaging system consists of 32 antennas positioned in a cylindrical setup inside a measurement tank as seen in Fig. 1 and is designed for operating in the frequency domain from 300 MHz to 3 GHz. During a measurement with the system, each antenna in turn acts as a transmitter while the remaining 31 antennas act as receivers, yielding a total of 992 measurements of amplitude and phase.

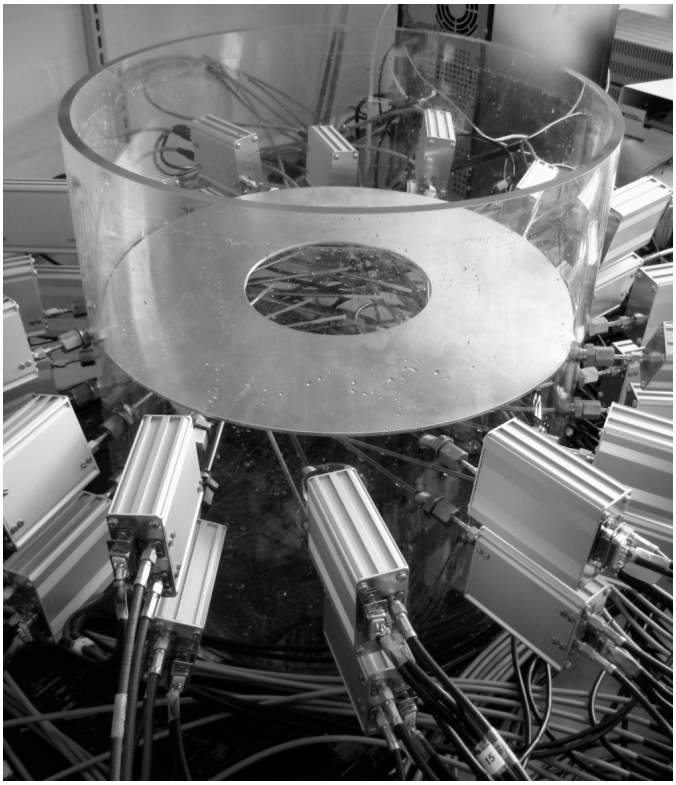

Fig. 1. Photo of the imaging system. The 32 horizontally oriented antennas are organized in a cylindrical setup to obtain coverage of the entire imaging domain.

The tank is filled with a glycerin-water coupling liquid, which mimics the constitutive parameters of the breast, thereby maximizing the coupling of energy from the antennas to the interior of the breast. By changing the glycerin-to-water ratio, the properties of the liquid can be adjusted to fit a large range of the reported average values for breast tissue [3], [9].

The liquid is lossy which means that the reflections from the sides of the measurement tank is reduced to a level where they become insignificant. This implies that the system may be modelled as being positioned in a homogeneous background with constitutive parameters equal to that of the coupling liquid.

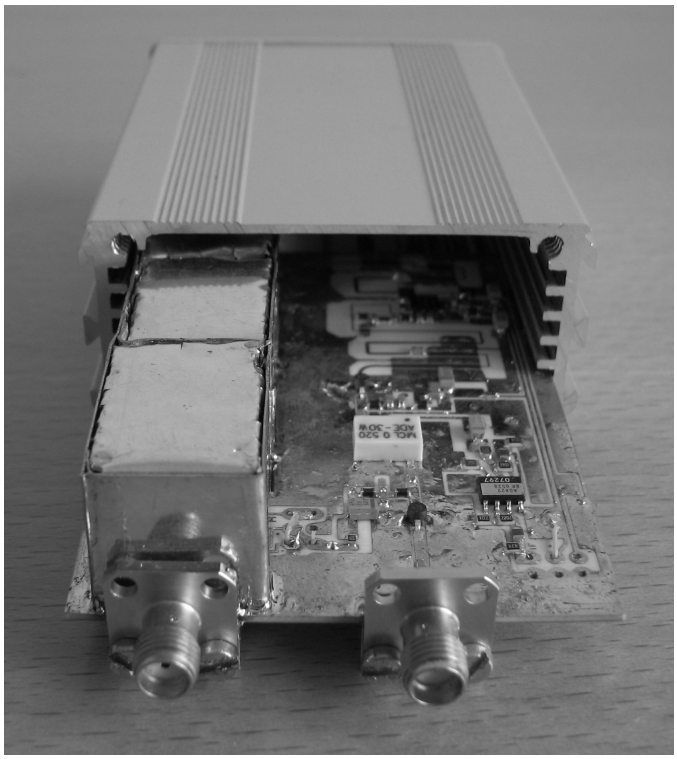

Fig. 2. Photo of an opened transceiver module. The switches are enclosed in a shielding structure to avoid leakage from the transmit to the receive channel.

In Fig. 1, a metal lid is positioned immediately above the antennas. In the examination system, the measurement tank will be cut off at this level allowing for the patient to lie prone on an exam bed with her breast suspended through the aperture in the lid. The metallic lid assures that the boundary towards the chest of the patient is known and thus easier to incorporate into the imaging algorithm.

The antennas used in the system are of a simple monopole type which has previously been applied for microwave imaging [10], [11]. This type of antenna is relatively broadband when positioned in the lossy coupling liquid and thus allows for operation in the entire frequency band of the imaging system. The simplicity of the antennas implies that they are both easy to manufacture and computationally inexpensive to model.

III. Microwave Hardware

To facilitate a short overall measurement time, each antenna has been equipped with its own transceiver module which has two functions: To allow duplexing between transmit and receive mode for each antenna and to provide conversion of the low-amplitude radio-frequency (RF) signal used for the imaging to a high-amplitude intermediate-frequency (IF) signal which is less susceptible to external noise sources. The modules can be seen attached to the end of the antennas in Fig. 1 and a photo of a transceiver module is shown in Fig. 2.

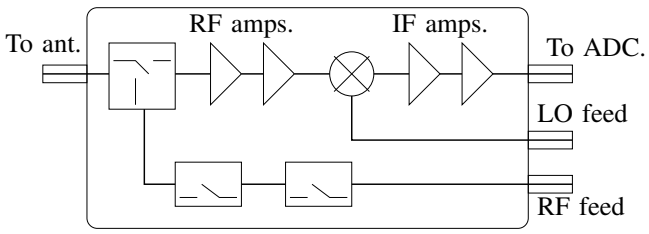

Fig. 3. Block diagram of the transceiver module. Two single-pole single-throw and one single-pole double-throw switch are applied to obtain the necessary isolation between the transmit and receive channel.

A block diagram of the layout of the transceiver modules is shown in Fig. 3. Each transceiver module contains a set of switches to allow the antennas to operate in either transmit or receive mode and amplifiers and mixers which allow to down-convert the frequency of the received signal to 1 kHz with an amplitude in the range 1 – 5 volts. The relatively low frequency and high amplitude of the IF signal implies that the connection from the individual transceiver modules to the analog-to-digital converter is less critical than if the RF signals measured by the antennas were to be transmitted all the way to a central down-converter.

Due to the losses in the coupling liquid, the signals received by the antennas are very low, especially at the higher frequencies where the level of the received signals may be as much as 130 dB below that of the transmitted in the upper region of the frequency spectrum. This implies that a high isolation between the transmit and receive channels in the transceiver module is required. This is achieved by using three individual switches (two single-pole single throw and one single-pole double throw) in the transceiver modules, each encased in its own shielding structure. The result is a total isolation of approximately 140 dB between the two channels.

The RF-amplification stage consists of a low-noise amplifier with a gain of 25 dB followed by a standard RF amplifier with a gain of 22 dB. Following the mixer, the IF signal is passed through two-stage amplifier with a total gain of 59 dB. The overall performance of the transceiver module when operating in receive mode (i.e. from antenna terminal to IF output) is a gain of 97 dB and a 2.3 dB noise figure and a noise floor below -140 dBm.

The IF output of the modules are fed to a 32 channel analog-to-digital converter (ADC). The ADC is capable of simultaneously sampling 8 channels with a sampling frequency of 100 kHz. For each channel, $10,000$ samples are used and a digital third-order band-pass filter with a bandwidth of 200 Hz is applied to filter out any higher-order components in the signal and reduce the noise floor.

The imaging algorithm requires not only the amplitude but also the phase of the signals to be measured. To ensure a fixed reference for the measurement of the phase, the signal which leaks through the single-pole double-throw switch in the transmitting module is measured with one of the 8 simultaneously applied channels, providing a reference for the phase of the

received signal.

The 18 bit ADC used in the system samples the input signals in the range from -5 to +5 volts. To ensure that this range is utilized to its maximum, the amplitude of the RF signal is adjusted in such a way that the amplitude of the IF signals has an amplitude between 1 and 5 volts. Because of the losses in the coupling liquid, the amplitude of the signals measured by the antennas close to the receiver may be much lower than that of the signals measured by antennas on the opposite side of the imaging system. Hence, the receiving antennas are divided into groups depending on their position relative to the transmitter. Using this approach, the amplitude RF signal feeding the transmitting antenna can be adjusted in such a way that the seven[1] signals which are measured simultaneously are all within the optimum range.

A complete measurement in with 32 transmitters with 31 receivers each takes just under 50 seconds to complete, including the time needed to switch between different transmitters and adjust the transmitting power.

IV. Imaging Algorithm

To reconstruct the distribution of constitutive electromagnetic properties of the breast, a hemispherical imaging domain with a radius of 7.5 cm is introduced in the center of the imaging system, immediately below the aperture through which the breast of the patient is to be suspended. This is illustrated in Fig. 4. The domain is discretized into cubic cells and in the individual cells, the constitutive parameters are assumed constant. The size of the cells are determined on the basis of the expected minimum expected size of the scatterer as well as on the wavelength in the coupling medium. In a typical setup, a side length of 5 mm is used.

To allow for the algorithm to include the effects of the chest wall of the patient being present above the aperture in the metallic lid, the imaging domain is extended to cover a 1 cm high cylindrical region with radius 7.5 cm positioned immediately above the aperture. It has been found that the effects of scatterers outside this region has virtually no influence on the measured signals. Hence, the region above the lid outside of this cylindrical region is assumed to have the same constitutive parameters as the coupling liquid.

The distribution of constitutive parameters in the imaging domain is reconstructed using an iterative Newton algorithm in which the nonlinear inversion problem

$$\underline{k}^2 = \operatorname{argmin}\left\{\underline{S}^{\text{meas}} - \underline{S}^{\text{calc}}(\underline{k}^2)\right\} \tag{1}$$

is solved.

In this expression, the vector $\underline{S}^{\text{meas}}$ contains the measured signals while the vector $\underline{S}^{\text{calc}}$ contains the simulated signals for the distribution of squared complex wave numbers in the imaging domain given by the vector $\underline{k}^2$. The squared complex wave number k^2 of the individual cell is given by its permittivity ϵ and conductivity σ as

$$k^2(\boldsymbol{r}) = \omega^2\mu_0\epsilon(\boldsymbol{r}) + i\omega\mu_0\sigma(\boldsymbol{r}) \tag{2}$$

[1]Plus the reference from the transmitter, i.e., eight in total.

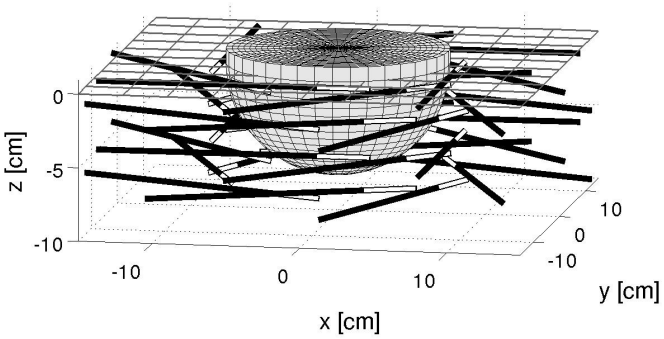

Fig. 4. Schematic of the imaging domain and the setup modeled in the forward solver. The imaging domain consists of a hemispherical region beneath the metallic lid and a cylindrical region with a height of 1 cm above the aperture in the lid. Since the antennas are positioned beneath the lid, 0.5 cm from the edge of the 15 cm diameter aperture, scatterers above the metallic lid has virtually no effect on the measured signals. In the standard configuration of the forward solver, the imaging domain is divided into 5 mm cubic cells, the antennas are modeled in full, and the metallic lid is included in the model.

assuming the time notation $\mathrm{e}^{-i\omega t}$. Herein, ω is the angular frequency, μ_0 is the free-space permeability and $\boldsymbol{r}$ is a position vector indicating the position of the cell.

Both the calculated and measured signals are represented using the log-amplitude unwrapped phase formulation first introduced for microwave imaging in [12]. Using this formulation, the elements of the two vectors $\underline{S}^{\text{meas}}$ and $\underline{S}^{\text{calc}}$ are given by the difference in the logarithm of the signal measured or calculated with an object inserted in the imaging system and the signal obtained with an empty imaging system. This yields a complex number given by the difference

$$S_{lp} = \log S_{\text{obj}} - \log S_{\text{empty}} \tag{3a}$$

in which the real part is the difference in the logarithm of the amplitudes

$$S_l = \log|S_{\text{obj}}| - \log|S_{\text{empty}}| \tag{3b}$$

and the imaginary part is the difference in (unwrapped) phase

$$S_p = \angle S_{\text{obj}} - \angle S_{\text{empty}}. \tag{3c}$$

This is different from the more widely used real-imaginary formulation in which the elements of the vectors are simply given by the difference between the signals measured with and without and object inserted in the imaging domain

$$S_{ri} = S_{\text{obj}} - S_{\text{empty}}. \tag{4}$$

The advantage of using the log-amplitude unwrapped phase formulation instead of the real-imaginary formulation is three fold. First, the use of the logarithm allows for an easy calibration of the signal level between the measured and the calculated signals as described in [13].

Second, the use of the difference in the logarithm of the amplitude implies that large relative changes in the signal levels are given more weight in the reconstruction. This is different from the real-imaginary formulation in which emphasis is put on large absolute changes. This difference is particularly pronounced when doing microwave imaging in lossy materials where the signals measured with the antennas on the opposite side of the imaging system from the transmitter are attenuated much more than the signals measured with the antennas in the vicinity of the transmitting antenna. Hence, an algorithm in which the weight is put on the absolute instead of the relative changes in the signal levels will to a large extent ignore the measurements made with the receivers on the opposite side of the imaging system. This is significant because, as described in [14], the measurements made with the antennas on the opposite side of the imaging system holds more information than the measurements made with antennas close to the transmitter.

Third and finally, the use of the unwrapped phase allows for the reconstruction to use several Riemann sheets whereas an algorithm based on the simple difference in the measured responses are constrained to a single Riemann-sheet. This is useful in breast imaging where the relatively large breast often results in phase changes outside of the region $\pm\pi$ covered by a single Riemann sheet. In order to be able to use multiple Riemann sheets, the phases of both the measured and the calculated signals need to be unwrapped. This unwrapping requires a minimum of additional computation and is described in details in [12].

In each iteration of the Newton algorithm, a forward problem is solved using a Method of Moments (MoM) code and the distribution of the distribution of constitutive parameters given by the vector $\underline{k}_n^2$ with n indicating the iteration number. The antennas are modelled in full in the forward model and the metallic lid is also included. This implies that any changes in the radiation patterns of the antennas caused by the presence of the breast in the imaging domain will be included in the forward model.

The MoM code used in the reconstruction algorithm has been augmented with the adaptive integral method and higher-order basis functions [15]. This is especially useful for reducing the computational cost of including the antennas and the metallic lid in the forward model.

After the forward problem has been solved to determine the elements of $\underline{S}_{\text{calc}}$, the Jacobian matrix of the problem is calculated. Since the MoM algorithm not only determines the field at the antennas but also the field in the imaging domain, the Jacobian matrix can be found in a computationally inexpensive matrix-product computation using the adjoint method [16].

The update vector $\underline{\Delta k}^2$ can then be found using

$$\underline{\Delta k}_n^2 = \operatorname{argmin} \left\{ \underline{\underline{J}}_n \underline{k}_n^2 - \left(\underline{S}^{\text{meas}} - \underline{S}^{\text{calc}}(\underline{k}_n^2) \right) \right\} \quad \text{subj. to regularization.} \tag{5}$$

Choosing the correct regularization scheme is important both for reducing the number of Newton iterations needed for the algorithm to converge and to achieve an image with high resolution and low artifact level. In [17] it was shown that the best results were obtained using an over-regularized solution of the linear problem in (5). It is, however, not a trivial task to determine the optimum regularization scheme for the imaging algorithm.

In the imaging algorithm currently implemented, the conjugated gradient least squares algorithm [18] is used in combination with a two-step Euclidean-distance algorithm similar to that described in [19] and a model-trust region approach [20].

After the update vector has been determined, the distribution of constitutive parameters is updated using

$$\underline{k}_{n+1}^2 = \underline{k}_n^2 + \underline{\Delta k}_n^2. \tag{6}$$

Typically, the reconstruction algorithm converges within 8 – 12 Newton iterations. The most time consuming part of the Newton algorithm is the solution of the forward problem using the MoM solver. Each iteration of the Newton algorithm requires approximately half an hour to complete when the standard configuration of the forward model is used. Of this time, the solution of the forward problem takes more than 95%.

The time needed for solving the forward problem can be reduced significantly by reducing the complexity of the problem. In particular, enlarging the cells (and thereby reducing the number of cells) in the imaging domain, modeling the antennas as Hertzian dipoles, or excluding the metal lid from the model will reduce the complexity considerably. This reduction is, however, obtained at the expense of a less accurate model of the physical problem and thus results in a degradation of the quality of the reconstructed images.

V. Conclusion

In this paper, the imaging system currently being developed at the Technical University of Denmark was described. This included a presentation of the overall imaging setup, the microwave hardware, and the imaging algorithm.

At the conference, the performance of the imaging system will be illustrated using phantom measurements and the effects of changing the configuration of the system, such as the operating frequency, the number of samples used by the ADC, and the different parameters of the imaging algorithm, will be discussed.

References

[1] W. T. Joines, Y. Zhang, C. Li, and R. L. Jirtle, "The measured electrical properties of normal and malignant human tissues from 50 to 900 MHz," *Medical Physics*, vol. 21, no. 4, pp. 547–50, 1994.

[2] S. P. Poplack, T. D. Tosteson, W. A. Wells, B. W. Pogue, P. M. Meaney, A. Hartov, C. A. Kogel, S. K. Soho, J. J. Gibson, and K. D. Paulsen, "Electromagnetic breast imaging: Results of a pilot study in women with abnormal mammograms," *Radiology - Radiological Society of North America*, vol. 243, no. 2, pp. 350–359, 2007.

[3] M. Lazebnik, D. Popovic, L. McCartney, C. B. Watkins, M. J. Lindstrom, J. Harter, S. Sewall, T. Ogilvie, A. Magliocco, T. M. Breslin, W. Temple, D. Mew, J. H. Booske, M. Okoniewski, and S. C. Hagness, "A large-scale study of the ultrawideband microwave dielectric properties of normal, benign and malignant breast tissues obtained from cancer surgeries," *Physics in Medicine and Biology*, vol. 52, no. 20, pp. 6093–6115, 2007.

[4] M. Klemm, I. J. Craddock, J. Leendertz, A. Preece, and R. Benjamin, "Experimental and clinical results of breast cancer detection using UWB microwave radar," *Proceedings of the IEEE Antennas and Propagation Society International Symposium, 2008*, 2008.
[5] W. C. Khor, H. Wang, M. E. Bialkowski, A. Abbosh, and N. Seman, "An experimental and theoretical investigation into capabilities of a UWB microwave imaging radar system to detect breast cancer," *EUROCON, 2007. The International Conference on Computer as a Tool*, pp. 771–776, 2007.
[6] T. Williams, J. Sill, and E. Fear, "Breast surface estimation for radar-based breast imaging systems," *IEEE Transactions on Biomedical Engineering*, vol. 55, no. 6, pp. 1678–1686, 2008.
[7] A. Fhager, P. Hashemzadeh, and M. Persson, "Reconstruction quality and spectral content of an electromagnetic time-domain inversion algorithm," *IEEE Transactions on Biomedical Engineering*, vol. 53, no. 8, pp. 1594–1604, 2006.
[8] H. Jiang, C. Li, D. Pearlstone, and L. Fajardo, "Ultrasound-guided microwave imaging of breast cancer: tissue phantom and pilot clinical experiments," *Medical Physics*, vol. 32, no. 8, pp. 2528–35, 2005.
[9] P. Meaney, M. Fanning, T. Raynolds, C. Fox, Q. Fang, C. Kogel, S. Poplack, and K. Paulsen, "Initial clinical experience with microwave breast imaging in women with normal mammography," *Academic Radiology*, vol. 14, no. 2, pp. 207–218, 2007.
[10] P. Meaney, K. Paulsen, A. Hartov, and R. Crane, "An active microwave imaging system for reconstruction of 2-D electrical property distributions," *IEEE Transactions on Biomedical Engineering*, vol. 42, no. 10, pp. 1017–1026, 1995.
[11] P. Hashemzadeh, A. Fhager, L. Baath, and M. Persson, "Experimental results of an optimization approach to two-dimensional time domain electromagnetic inverse problem with application to microwave breast tomography," *Proceedings of the 3rd IASTED International Conference on Biomedical Engineering, 2005*, pp. 192–196, 2005.
[12] P. Meaney, K. Paulsen, B. Pogue, and M. Miga, "Microwave image reconstruction utilizing log-magnitude and unwrapped phase to improve high-contrast object recovery," *IEEE Transactions on Medical Imaging*, vol. 20, no. 2, pp. 104–116, 2001.
[13] P. Meaney, K. Paulsen, and J. Chang, "Near-field microwave imaging of biologically-based materials using a monopole transceiver system," *IEEE Transactions on Microwave Theory and Techniques*, vol. 46, no. 1, pp. 31–45, 1998.
[14] P. M. Meaney, T. Zhou, S. A. Geimer, and K. D. Paulsen, "Implications of reduced measurement data sets on overall microwave tomographic image quality," *Proceedings of the European Conference on Antennas and Propagation EuCAP, 2007*, 2007.
[15] O. S. Kim and P. Meincke, "Adaptive integral method for higher order method of moments," *IEEE Transactions on Antennas and Propagation*, vol. 56, no. 81, pp. 2298–2305, 2008.
[16] P. Meaney, Q. Fang, M. Fanning, S. Pendergrass, T. Raynolds, C. Fox, and K. Paulsen, "Microwave breast imaging with an under-determined reconstruction parameter mesh," *Proceedings of the IEEE International Symposium on Biomedical Imaging: Macro to Nano, 2004*, pp. 1369–1372, 2004.
[17] T. Rubæk, P. M. Meaney, P. Meincke, and K. D. Paulsen, "Nonlinear microwave imaging for breast-cancer screening using Gauss-Newton's method and the CGLS inversion algorithm," *IEEE Transactions on Antennas and Propagation*, vol. 55, no. 8, pp. 2320–2331, 2007.
[18] P. C. Hansen, *Rank-Deficient and Discrete Ill-Posed Problems: Numerical Aspects of Linear Inversion*, ser. Monographs on Mathematical Modeling and Computation. SIAM, 1998.
[19] P. Meaney, E. Demidenko, N. Yagnamurthy, D. Li, M. Fanning, and K. Paulsen, "A two-stage microwave image reconstruction procedure for improved internal feature extraction," *Medical Physics*, vol. 28, no. 11, pp. 2358–2369, 2001.
[20] J. E. Dennis and R. B. Schnabel, *Numerical Methods for Unconstrained Optimization and Nonlinear Equations*, ser. Classics in Applied Mathematics, R. E. O'Malley, Ed. Philadelphia: SIAM - Society for Industrial and Applied Mathematics, 1996.